Excited-state dynamics in the low-phonon materials $Er^{3+}:BaY_2F_8$ and $Cs_3Er_2Br_9$

M. Pollnau, W. Lüthy, and H. P. Weber
Institute of Applied Physics, University of Bern, Sidlerstrasse 5, CH-3012 Bern, Switzerland

K. Krämer and H. U. Güdel
Institute of Inorganic Chemistry, University of Bern, Freiestrasse 3, CH-3009 Bern, Switzerland

R. A. McFarlane
Hughes Research Laboratories, 3011 Malibu Canyon Road, Malibu, California 90265

Abstract

By measuring ground-state absorption (GSA), fluorescence, and excited-state absorption (ESA) at the wavelength region around 550 nm the population dynamics in $Er^{3+}:BaY_2F_8$ and $Cs_3Er_2Br_9$ are investigated. The excitation dynamics of $Er^{3+}:BaY_2F_8$ are comparable with those in other fluoride or oxide materials. In $Cs_3Er_2Br_9$ the smaller Stark splitting of the levels shifts the wavelengths of the green emission and parasitic ESA off resonance. It enhances, however, ground-state reabsorption. Upconversion leads to significant green fluorescence from the $^2H_{9/2}$ level. Multiphonon transitions do not contribute to the population dynamics in $Cs_3Er_2Br_9$.

Key Words

Rare earth doped materials, Laser materials, Energy transfer, Spectroscopy-fluorescence and luminescence.

Introduction

The development of compact blue and green emitting crystal lasers [1,2] pumped by infrared diodes has become interesting for applications in the fields of data storage and display. The BaY_2F_8 and $Cs_3Er_2Br_9$ crystals which are investigated in this paper are candidates as host materials for green laser emission. Phonon energies of 415 cm^{-1} in BaY_2F_8 [3] and 190 cm^{-1} in $Cs_3Er_2Br_9$ [4] lead to a long lifetime of the $^4S_{3/2}$ upper laser level in erbium. The measurement of GSA, fluorescence, and ESA provides important information on the population dynamics in $Er^{3+}:BaY_2F_8$ and $Cs_3Er_2Br_9$. Owing to different size and weight of the ligands the excitation mechanisms, fluorescence properties, ESA and stimulated-emission (SE) dynamics are completely different in the bromide compared with the fluoride material. Systematic differences in wavelength ranges, multiphonon relaxations, and interionic processes are discussed.

Experimental

A pump- and probe-beam technique is used for the measurement of quasi-cw-pumped ESA spectra. The broadband probe light is transmitted through the sample, spectrally analyzed with a monochromator (resolution 0.2 nm), and detected by an optical photodiode. The difference of the transmitted probe-beam intensities I_p and I_u with and without 800-nm excitation of the sample is measured in double-lock-in technique [5,6,7]. With dopant concentration n_0, excitation density n_e, sample thickness d, and ground-state-absorption (GSA) cross section σ_{GSA}, the cross section σ_{ESA} - σ_{SE} originating from level i at wavelength λ is calculated using the equation [8]

$$\Sigma_i [(n_i / n_e) (\sigma_{ESA,i} - \sigma_{SE,i})] = \ln (I_u / I_p) / (n_e d) + \sigma_{GSA}. \quad (1)$$

The GSA and fluorescence spectra are also measured with this arrangement and the same spectral resolution with a normal lock-in technique.

Results and Discussion

The energy level scheme of erbium, the intrinsic lifetimes of the various metastable levels in the different host materials, the excitation mechanisms

OSA TOPS on Advanced Solid-State Lasers, 1996
Vol. 1, Stephen A. Payne and Clifford Pollock (eds.)

under 800-nm radiation, and the investigated transitions are indicated in Fig. 1 for Er^{3+}:BaY_2F_8 and in Fig. 2 for $Cs_3Er_2Br_9$. Lifetimes were measured in Er^{3+}(1%):BaY_2F_8 [3] and Er^{3+}(1%):$Cs_3Lu_2Br_9$ [4].

The erbium ions are excited into the $^4I_{9/2}$ level. The excitation dynamics of Er^{3+}:BaY_2F_8 are comparable with those in other fluoride or oxide materials [7,8]. Multiphonon relaxations populate the $^4I_{11/2}$ and $^4I_{13/2}$ levels. Interionic upconversion and multiphonon relaxations populate the $^4S_{3/2}$ level which leads to emission $^4S_{3/2} \rightarrow {}^4I_{15/2}$ at 550 nm (Fig. 3b). In BaY_2F_8 ground-state reabsorption on the green laser wavelength at 550 nm is small (Figs. 3a-b). However, the green emission has a spectral overlap with parasitic ESA $^4I_{13/2} \rightarrow {}^2H_{9/2}$ (Figs. 3b-c). This ESA may limit green laser operation $^4S_{3/2} \rightarrow {}^4I_{15/2}$ to cryogenic temperatures [9]. The strong ESA $^4I_{11/2} \rightarrow {}^2K_{15/2}$ +

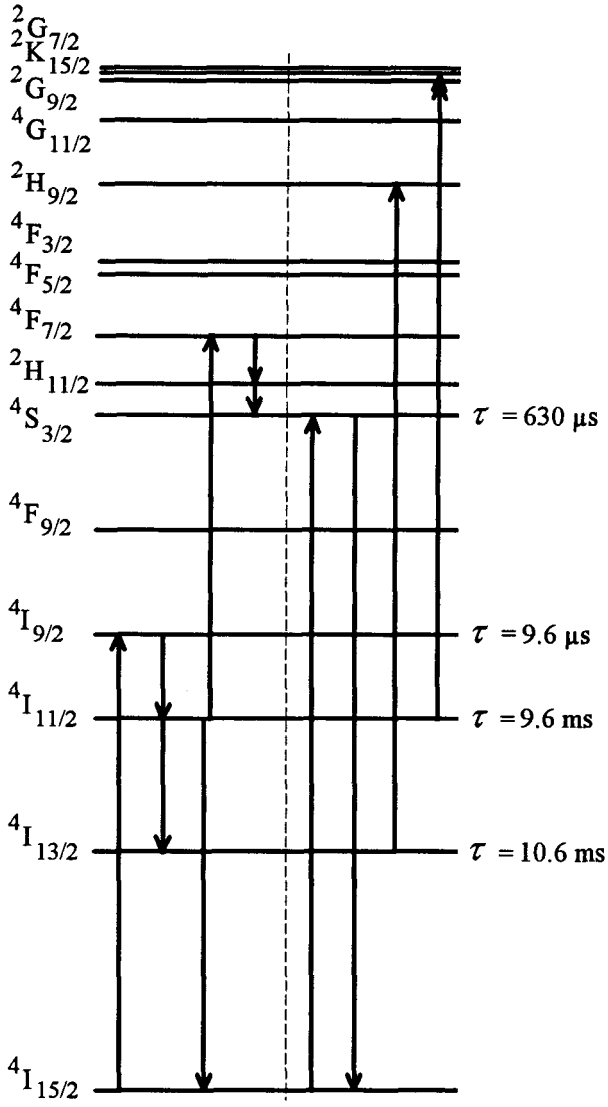

Figure 1. Energy-level diagram indicating the excitation mechanisms (left-hand side) and the detected transitions (right-hand side) in Er^{3+}(7.5%):BaY_2F_8. The erbium ions are excited into the $^4I_{9/2}$ level. Multiphonon relaxations populate the $^4I_{11/2}$ and $^4I_{13/2}$ levels. Interionic upconversion and multiphonon relaxations populate the $^4S_{3/2}$ level. Investigated is the overlap of GSA to $^4S_{3/2}$, fluorescence from $^4S_{3/2}$, and parasitic ESA from $^4I_{13/2}$ and $^4I_{11/2}$ at the laser wavelength 550 nm.

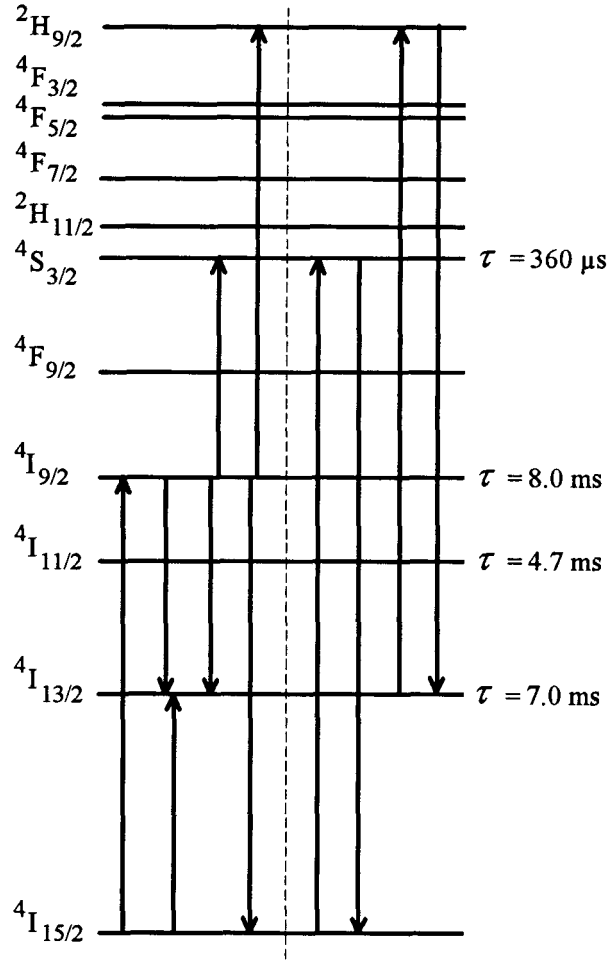

Figure 2. Energy-level diagram indicating the excitation mechanisms (left-hand side) and the detected transitions (right-hand side) in $Cs_3Er_2Br_9$. The erbium ions are excited into the $^4I_{9/2}$ level. Cross-relaxation and upconversion processes from $^4I_{9/2}$ populate the $^4I_{13/2}$, $^4S_{3/2}$, and $^2H_{9/2}$ levels. The $^4I_{11/2}$ level is not significantly populated under 800-nm excitation. Investigated is the overlap of GSA to $^4S_{3/2}$, fluorescences from $^4S_{3/2}$ and $^2H_{9/2}$ as well as ESA from $^4I_{13/2}$ at the possible laser wavelength 550 nm.

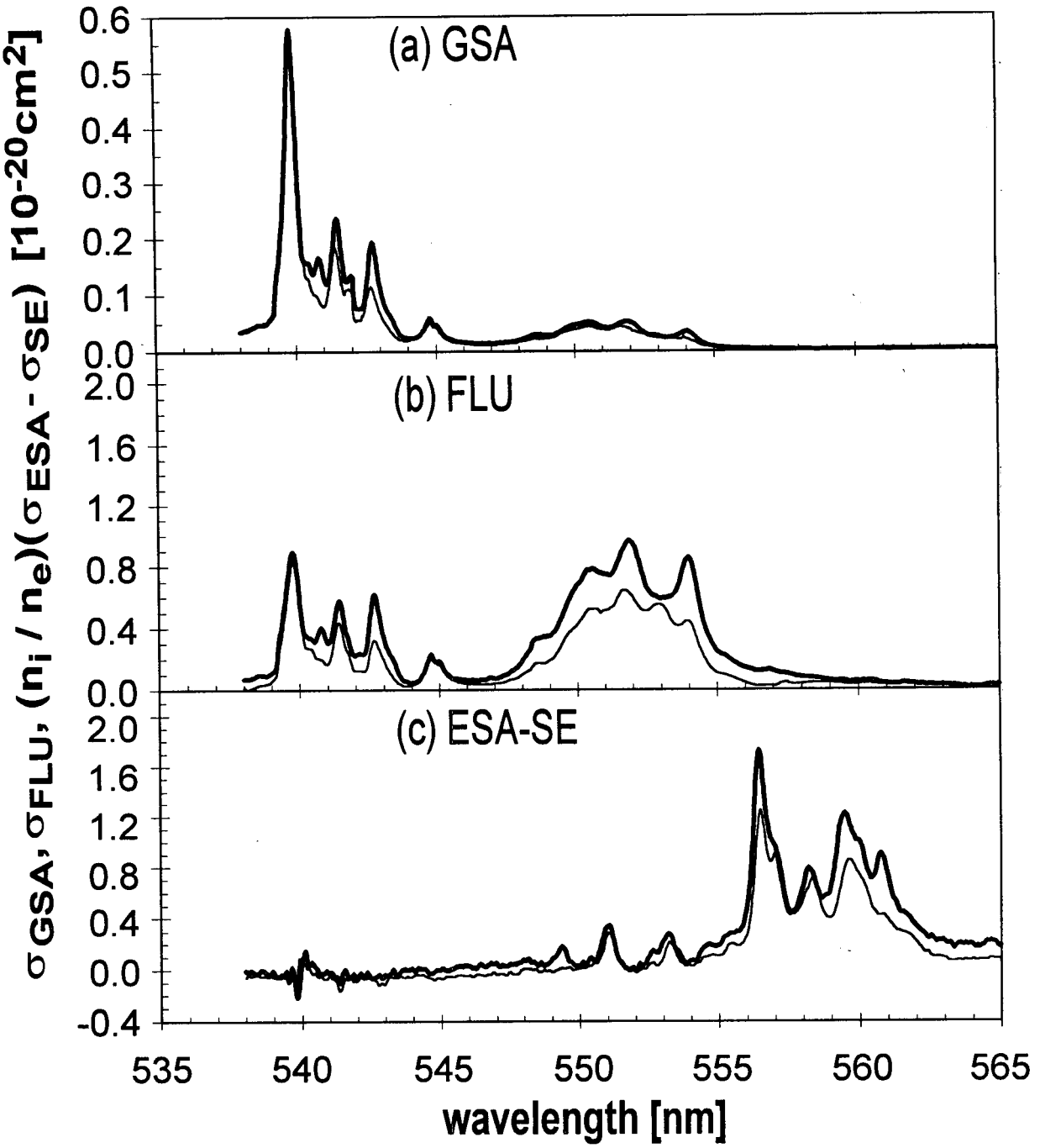

Fig. 3. Polarized spectra at the laser wavelength 550 nm of Er(7.5%):BaY_2F_8, **E** || y (thick line) and **E** || z (thin line): (a) GSA $^4I_{15/2} \rightarrow {}^4S_{3/2}$, (b) fluorescence $^4S_{3/2} \rightarrow {}^4I_{15/2}$, (c) ESA $^4I_{13/2} \rightarrow {}^2H_{9/2}$ and $^4I_{11/2} \rightarrow {}^2K_{15/2} + {}^2G_{9/2}$. The labeling of the crystal axes is equivalent to the designations specified in [10].

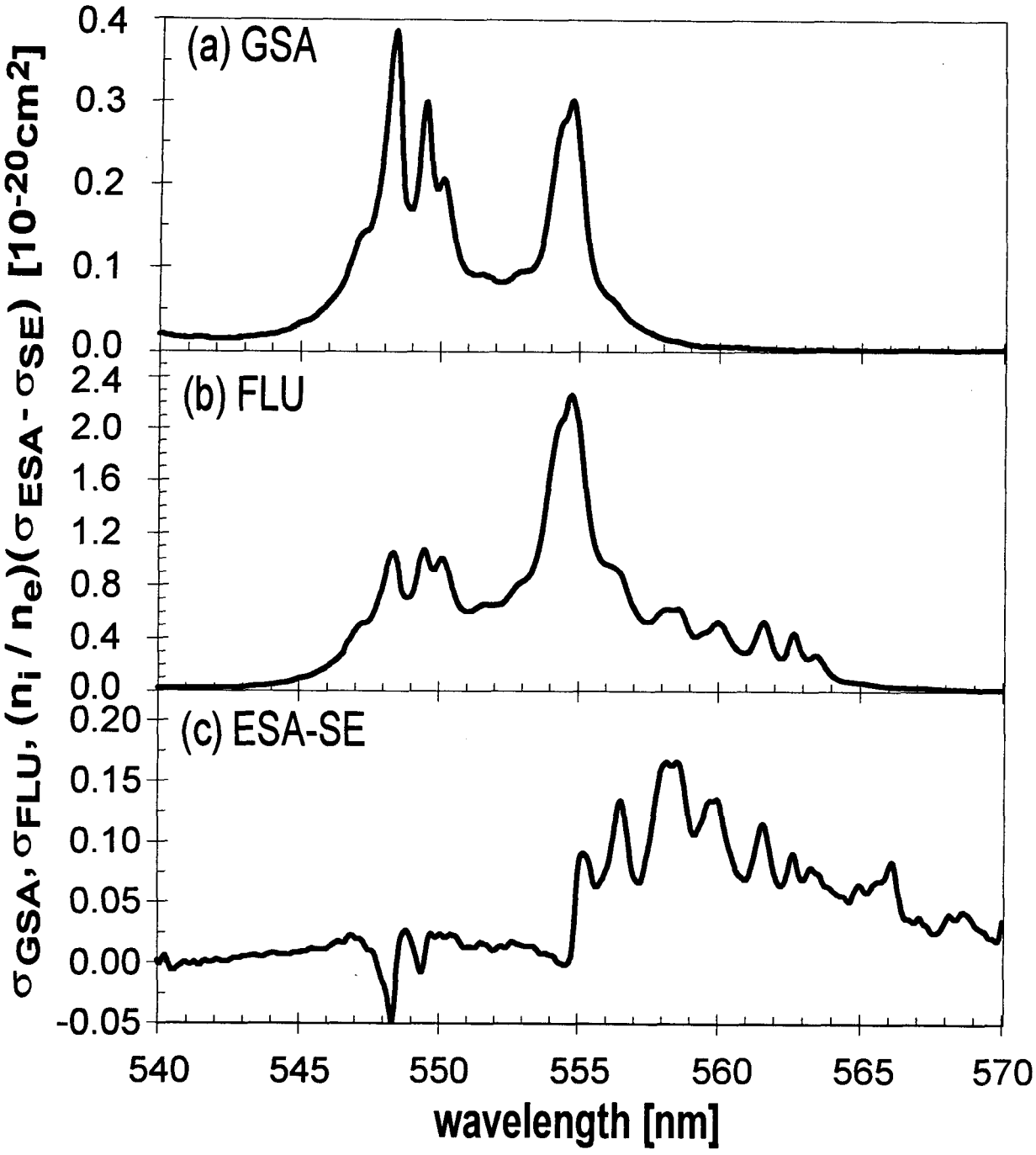

Fig. 4. Arbitrarily polarized spectra of $Cs_3Er_2Br_9$ at the possible laser wavelength 550 nm: (a) GSA $^4I_{15/2} \rightarrow {}^4S_{3/2}$, (b) fluorescences $^4S_{3/2} \rightarrow {}^4I_{15/2}$ and $^2H_{9/2} \rightarrow {}^4I_{13/2}$, (c) ESA $^4I_{13/2} \rightarrow {}^2H_{9/2}$.

$^2G_{9/2}$ at 560-570 nm has no overlap with green emission (Figs. 3b-c). The originating levels of the different ESA transitions are known from time-resolved ESA measurements in Er^{3+}:$YAlO_3$ [8].

Differences between $Cs_3Er_2Br_9$ and BaY_2F_8 are mainly induced by the larger size and higher atomic weight of the bromide ions compared with the fluoride ions. The larger size widens the lattice and weakens the electric crystal field that is induced at the rare-earth site by the Br^- ligands. Thus the Stark splitting of every level is reduced. The high atomic weight limits the energetic spectrum of the lattice vibrations which results in the almost complete absence of multiphonon transitions even at room temperature. The close proximity of two erbium ions in the $Cs_3Er_2Br_9$ lattice [4], the high erbium concentration of $3.8x10^{21}$ cm^{-3}, and the long lifetimes of otherwise multiphonon-quenched levels lead to the occurrence of ion-ion interactions that are not observed in BaY_2F_8. The population mechanisms are, therefore, dominated by fluorescence decay as well as specific interionic upconversion and cross-relaxation processes.

In $Cs_3Er_2Br_9$ pumping the $^4I_{9/2}$ level does not lead to the population of the $^4I_{11/2}$ level via multiphonon relaxation. Instead, a considerable population is created in the pump level itself which is then subject to interionic energy transfer (Fig. 2). Cross-relaxation and upconversion processes populate the $^4I_{13/2}$ level. Upconversion processes populate the $^4S_{3/2}$ and $^2H_{9/2}$ levels.

The reabsorption of fluorescence $^4S_{3/2} \rightarrow {}^4I_{15/2}$ by parasitic ESA $^4I_{13/2} \rightarrow {}^2H_{9/2}$ is systematically avoided. Owing to the smaller Stark splitting there is no spectral overlap (Figs. 4b-c). The same mechanism is responsible, however, for a higher population of the terminating laser level and a smaller inversion on the laser transition in $Cs_3Er_2Br_9$ (Figs. 4a-b). The inverse process of the ESA, the green fluorescence $^2H_{9/2} \rightarrow {}^4I_{13/2}$, is observed in $Cs_3Er_2Br_9$ (Fig 4b), because the $^2H_{9/2}$ level is not quenched by multiphonon relaxation. The $^4I_{13/2}$ level is more highly populated than the $^2H_{9/2}$ level. The $^4I_{13/2} \leftrightarrow {}^2H_{9/2}$ transition is, therefore, detected as an ESA process in the ESA/SE spectrum (Fig. 4c). The strong ESA $^4I_{11/2} \rightarrow {}^2K_{15/2} + {}^2G_{9/2}$ observed at wavelengths longer than 560 nm in BaY_2F_8 (Fig. 3c) is completely missing in $Cs_3Er_2Br_9$ (Fig. 4c).

Conclusions

The ground-state-absorption, fluorescence, and excited-state-absorption spectra at the erbium laser wavelength 550 nm have been measured in BaY_2F_8 and $Cs_3Er_2Br_9$. Owing to the different size and weight of the anions the population mechanisms and the spectral properties at the green wavelength range are completely different in BaY_2F_8 and $Cs_3Er_2Br_9$. In $Cs_3Er_2Br_9$ the smaller Stark splitting of the levels shifts the wavelengths of the green emission and ESA from $^4I_{13/2}$ off resonance, but it is also responsible for a higher population of the terminating laser level and a smaller inversion on the possible laser transition. The population mechanisms and lifetimes are dominated by fluorescence decay as well as specific interionic upconversion and cross-relaxation processes that are not observed in BaY_2F_8. Multiphonon relaxations do not significantly contribute to the population dynamics in $Cs_3Er_2Br_9$.

Acknowledgment

This work was supported in part by the Swiss Priority Program "Optique" and by the U.S. Air Force Office of Scientific Research under Contract No. F49620-94-C-0018.

References

1. R. Brede, T. Danger, E. Heumann, G. Huber, and B. H. T. Chai, Appl. Phys. Lett. **63**, 729 (1993).
2. R. A. McFarlane, J. Opt. Soc. Am. B **11**, 871 (1994).
3. D. S. Knowles and H. P. Jenssen, IEEE J. Quantum Electron. **28**, 1197 (1992).
4. M. P. Hehlen, K. Krämer, H. U. Güdel, R. A. McFarlane, and R. H. Schwartz, Phys. Rev. B **49**, 12475 (1994).
5. S. Zemon, G. Lambert, W. J. Miniscalco, R. W. Davies, B. T. Hall, R. C. Folweiler, T. Wei, L. J. Andrews, and M. P. Singh, SPIE Vol. **1373**, 21 (1990).
6. J. Koetke and G. Huber, Appl. Phys. B **61**, 151 (1995).
7. T. Danger, J. Koetke, R. Brede, E. Heumann, G. Huber, and B. H. T. Chai, J. Appl. Phys. **76**, 1413 (1994).
8. M. Pollnau, E. Heumann, and G. Huber, Appl. Phys. A **54**, 404 (1992).
9. M. Pollnau, E. Heumann, and G. Huber, J. Lumin. **60+61**, 842 (1994).
10. K. M. Dinndorf, D. S. Knowles, M. Gojer, and H. P. Jenssen, "Principal axes for transitions in monoclinic crystals", OSA Proceedings on Advanced Solid State Lasers, Lloyd L. Chase and Albert A. Pinto, eds. (Optical Society of America, Washington, DC 1992), pp. 270-274.